

Gapped Excitations in the High-Pressure Antiferromagnetic Phase of URu₂Si₂

T.J. Williams,^{1,2,*} H. Barath,³ Z. Yamani,⁴ J.A. Rodriguez-Riviera,^{5,6} J.B. Leão,⁵
J.D. Garrett,⁷ G.M. Luke,^{1,7,8} W.J.L. Buyers,^{4,8} and C. Broholm^{3,5,†}

¹*Department of Physics and Astronomy, McMaster University, Hamilton, ON, Canada, L8S 4M1*

²*Quantum Condensed Matter Division, Neutron Sciences Directorate,
Oak Ridge National Lab, Oak Ridge, TN, 37831, USA*

³*Institute for Quantum Matter and Department of Physics and Astronomy,
Johns Hopkins University, Baltimore, MD, USA, 21218*

⁴*National Research Council, Chalk River Laboratories, Chalk River, ON, Canada, K0J 1J0*

⁵*NIST Center for Neutron Research, National Institute of Standards and Technology, Gaithersburg, MD, USA, 20899*

⁶*Department of Materials Science and Engineering,
University of Maryland, College Park, MD, USA, 20740*

⁷*Brockhouse Institute for Materials Science, McMaster University, Hamilton, ON, Canada, L8S 4M1*

⁸*Canadian Institute for Advanced Research, Toronto, Ontario, Canada, M5G 1Z8*

(Dated: February 11, 2021)

We report a neutron scattering study of the magnetic excitation spectrum in each of the three temperature and pressure driven phases of URu₂Si₂. We find qualitatively similar excitations throughout the (HOL) scattering plane in the hidden order and large moment phases, with no changes in the $\hbar\omega$ -widths of the excitations at the $\Sigma = (1.407, 0, 0)$ and $Z = (1, 0, 0)$ points, within our experimental resolution. There is, however, an increase in the gap at the Σ point from 4.2(2) meV to 5.5(3) meV, consistent with other indicators of enhanced antiferromagnetism under pressure.

PACS numbers: 78.70.Nx, 71.27.+a

The heavy fermion material URu₂Si₂ exhibits a specific heat anomaly at $T_0 = 17.5$ K indicative of a second order phase transition [1, 2]. Decades of research notwithstanding [3–6], an order parameter characterizing the putative symmetry breaking of the low temperature phase has not been identified. Neutron scattering does show antiferromagnetic order with an ordering wavevector $\mathbf{Q}_m = (1, 0, 0)$, but the small sample-averaged moment of $0.03 \mu_B$ [2], seems hard to reconcile with a change in entropy $\Delta S = 0.24R \ln 2$ [1] through the transition. This moment may even be intrinsic [7] or it may arise from heterogeneous inclusions of a large moment phase [8]. Spin fluctuations with a characteristic wave vector $(1 \pm \delta, 0, 0)$ ($\delta = 0.407(6)$) are observed in the paramagnetic (PM) phase, indicative of Fermi-surface nesting at the Σ point, which for URu₂Si₂ occurs for $\delta = \frac{1}{2}(1 - (a/c)^2) = 0.406$ ($a=4.128 \text{ \AA}$ and $c=9.534 \text{ \AA}$ at $T=4 \text{ K}$) [9]. Below T_0 , in the so-called ‘hidden order’ (HO) phase, these excitations become gapped as for a spin density wave transition and consistent with the specific heat anomaly, but without development of the attendant staggered magnetization.

Hydrostatic pressure of ~ 0.6 GPa replaces the HO phase with a large-moment antiferromagnetic (AF) phase with an ordered magnetic moment of $0.3 \mu_B$ [10, 11]. Here we show the gapped excitations at the $\Sigma = (1.407, 0, 0)$ and $Z = (1, 0, 0)$ points persist in the AF phase, albeit with an enhanced gap at the Σ point in the high pressure phase. Our results are not inconsis-

tent with previous experimental data [10, 12, 13], though they clearly show an inelastic signal at the Z point. Our expanded coverage of \mathbf{Q} - E space reveals a similarity between magnetic excitations in the two low temperature phases that was not previously appreciated.

High quality single crystals of URu₂Si₂ were grown by the Czochralski method in a tri-arc furnace. Three crystals with a total mass of approximately 37 g and an RRR ≈ 10 were coaligned in the (HOL) plane for the ambient pressure measurements. A single crystal with a mass of 1.66 g and an RRR = 15 was cut by spark erosion, aligned in the (HOL) plane, placed inside a 13-8Mo steel He-gas pressure vessel, and connected to a commercially available pressurizing intensifier through a heated high-pressure capillary. Following the procedure established in Ref. [11], the pressure was adjusted only at temperatures well above the helium melting curve and the capillary was heated during slow cooling of the cell to accommodate the contracting He gas, thus minimizing pressure loss and pressure inhomogeneities across the sample space. The pressure cell was cooled at constant pressure to the freezing point of helium. Through prior calibration measurements of the lattice parameters of highly oriented pyrolytic graphite crystals within the cell, the pressure reduction upon cooling following these procedures is less than 0.05 GPa. The neutron scattering measurements were performed on the Multi-Axis Crystal Spectrometer (MACS) at the NIST Center for Neutron Research, where a 20 MW reactor, a dedicated liquid H₂ moderator, and a doubly-focusing PG(002) monochromator provides an incident beam flux of $3.0 \times 10^8 \text{ n/cm}^2/\text{s}$ [14] for an initial energy $E_i = 5 \text{ meV}$. In the vicinity of (1,0,0), the in-plane resolution was 0.12 \AA^{-1} along L , 0.043 \AA^{-1} along

*Electronic address: williamstj@ornl.gov

†Electronic address: broholm@jhu.edu

H , and the out-of-plane resolution was 0.24 \AA^{-1} at zero energy transfer. All measurements were performed using a fixed $E_f = 5.054 \text{ meV}$, with an elastic energy resolution of 0.45 meV . Twenty detection channels permitted efficient mapping of inelastic scattering throughout the $(H0L)$ plane. Measurements were performed at ambient pressure and $T = 25 \text{ K}$ in the paramagnetic phase, at ambient pressure and $T = 2 \text{ K}$ in the hidden order phase, and at a pressure of $P = 1.02 \text{ GPa}$ and $T = 4 \text{ K}$ in the AF phase.

Phonon scattering near $(0,0,2)$ is visible in both the paramagnetic (Fig. 1(a)) and hidden order (Fig. 1(b)) phases. This allowed for normalization of the data so that we can provide absolute values of the scattering cross sections in each phase, which are consistent with previously published values [15]. To isolate scattering from URu_2Si_2 from that associated with the massive pressure cell and the helium pressure medium, a background was measured for the pressure cell with the sample exchanged by an equal volume of aluminum pressurized to 1.02 GPa . Due to the reduced neutron absorption of Al relative to URu_2Si_2 , this results in a slight over-subtraction and thus a difference signal with a small negative background value, as shown below. The scattering intensity under pressure was also subject to normalization using the $(0,0,2)$ structural Bragg peak, which showed the transmission of the pressure cell is 18%, consistent with direct measurements. Attributing all of the scattering at $(1,0,0)$ to magnetic scattering, the normalization yields a cross section for the $(1,0,0)$ magnetic Bragg peak of $0.36(9) \mu_B$, which is in good agreement with the previously reported ordered moment in the AF phase [10]. All data were corrected for the effects of higher order contamination on the monitor count rate [14].

The inelastic scattering cross section along high symmetry directions in the $(H0L)$ plane for the three different phases is shown in Fig. 1. The upper and middle panels show the momentum and energy transfer dependence of the magnetic scattering in the PM and HO phases, respectively, which are consistent with earlier findings [2, 9, 16]. There are substantial changes across the PM to HO phase transition. In the PM phase, the scattering takes the form of gapless ridges with most of the intensity at the Σ point though a ridge is also clearly discerned at the Z point. In the HO phase, well-defined gaps have opened at both the Z and Σ points, and the intensity at the Z point has increased. The lowest panel shows data in the AF phase. Due to the pressure cell the quality of these data is significantly reduced. Nonetheless, to within error in the AF phase, the overall Q - ω dependent scattering is qualitatively similar to that of the HO phase, though as seen in constant- Q cuts of the data, the gap at the Σ point is considerably enhanced.

Further comparisons between the three phases is made by examining the constant energy transfer slices through the $(H0L)$ zone data, shown in Fig. 2. The figure shows the average intensity in 1 meV -thick slices centered at 2 meV , 5 meV , 8 meV and 11 meV . For improved statis-

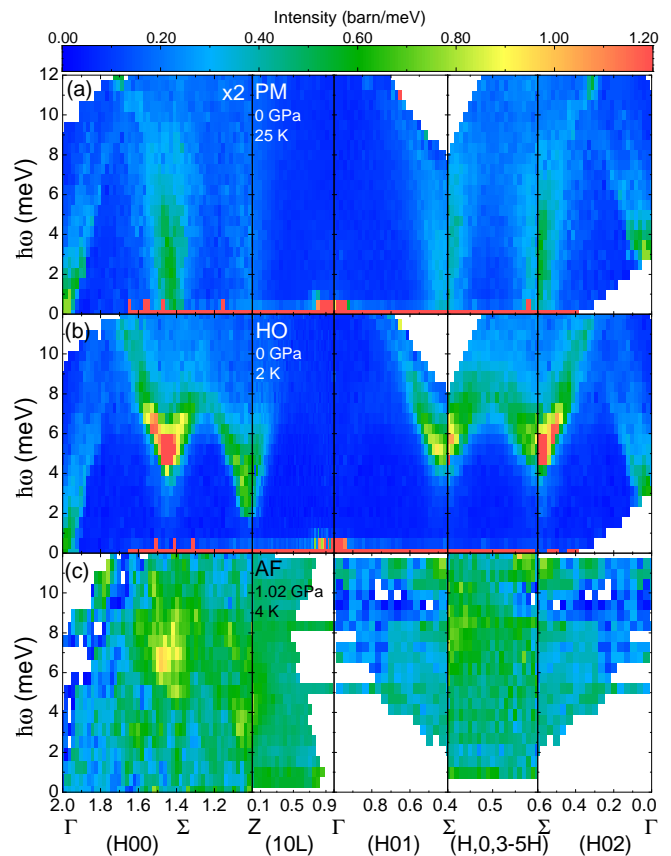


FIG. 1: (Color online) The scattering intensity as a function of energy and scattering vector along various high symmetry directions in the $(H0L)$ plane in the three phases studied: (a) at ambient pressure and 25 K , in the paramagnetic (PM) phase. For ease of viewing, the data has been scaled up by a factor of 2. The phonon at $(2,0,0)$ is visible, as are magnetic excitations at the Σ point. (b) Data collected at ambient pressure and 2 K , in the HO phase. (c) Data collected at 1.02 GPa and 4 K , in the AF phase. The scattering here looks qualitatively similar to the HO phase, albeit with a larger gap at the Σ point. The reduced statistical quality results from the reduced neutron transmission through the pressure cell and the subtraction of a strong background signal from the pressure cell and the solid helium pressure transmitting medium.

tics, we have symmetrized the data and present a single quadrant at each energy transfer. While intensity at the Σ point is present in all three phases, intensity at the Z point is mainly visible in the HO and AF phases. In the HO phase, there is considerably more spectral weight in all of the excitations compared to the PM phase. Comparing the HO and AF phase, we see in the 5 meV slice that the gap in the AF phase is larger at the Σ points. The Z and Σ modes have similar intensity at 8 meV within the AF phase compared to 5 meV in the HO phase. In the HO phase, the 8 meV data consists of smooth ridges, while well-defined reciprocal space intensity maxima are still visible at 8 meV in the AF data.

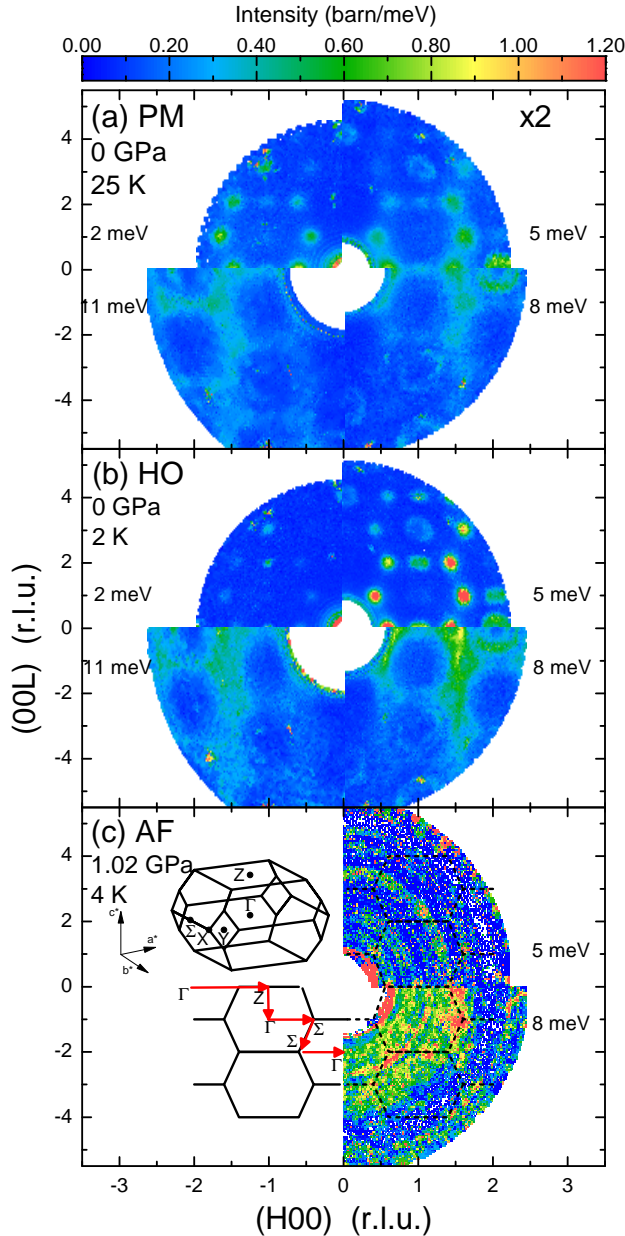


FIG. 2: (Color online) Constant energy slices in the $(H0L)$ plane in each of the three phases of URu_2Si_2 . Energies shown are 2 meV, 5 meV, 8 meV and 11 meV (clockwise from top left). The range of integration of energies for the slices was ± 0.5 meV and the bin size is 0.013 \AA^{-2} . The data in the PM phase (panel (a)) has been scaled up by a factor of 2, as in Fig. 1. The lower left of the figure shows the Brillouin zone of URu_2Si_2 , with the arrows indicating the directions shown in Fig. 1.

For a quantitative spectral analysis, the energy dependence of the scattering at Z and Σ in the three phases is shown in Fig. 3. These cuts were extracted from the same data that is shown in Fig. 1 and Fig. 2. Follow-

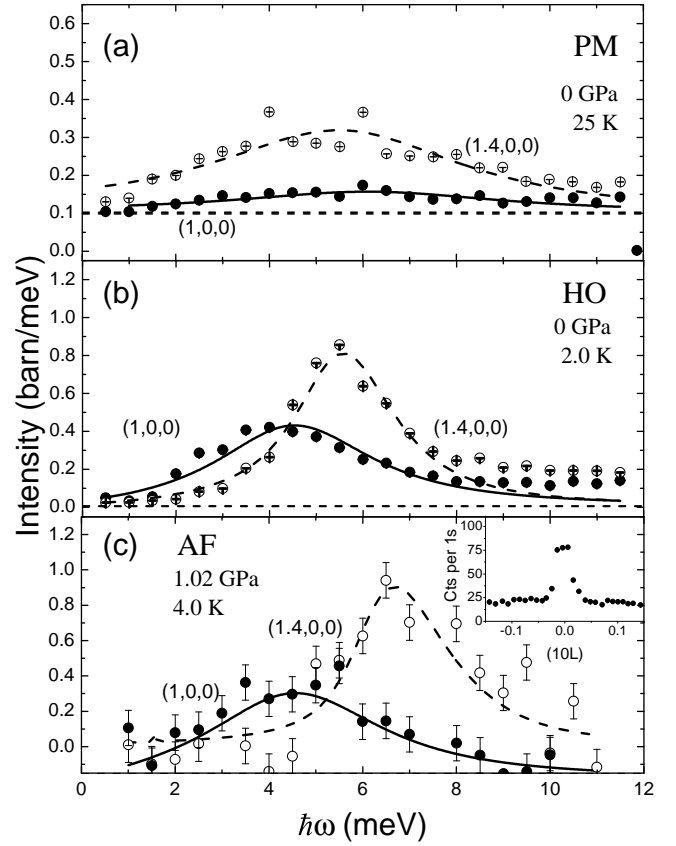


FIG. 3: (Color online) The energy-dependence of the scattering intensity for crystal momentum Z (filled circles) and Σ (open circles) in each phase. The error bars represent 1 standard deviation, σ . The lines are fits as described in the text, with the horizontal dashed lines showing the fitted background. (a) In the PM phase, a weak and broad spectrum of scattering is seen at Z , with a more pronounced but also broad peak at Σ . (b) In the HO phase, the scattering is more intense at both wave vectors and intensity at Σ has shifted to higher energy. (c) In the AF phase, both peaks are still present; the peak at $(1.4,0,0)$ has shifted to slightly higher energies. Note: the fitted background lies below the axis here, due to the subtraction described in the text. Inset: the scattering along $(10L)$ in the AF phase. When normalized, the peak intensity at $(1,0,0)$ corresponds to a sample averaged staggered moment of $0.36(9) \mu_B$.

ing the analysis of [17], the data in each phase was fit to the resolution-convoluted line shape associated with the following expression for the low temperature magnetic scattering cross section near the Z and Σ points:

$$\tilde{I}(\mathbf{Q}, \omega) = \frac{\mathcal{A}}{\epsilon(\mathbf{Q})} \cdot \frac{1 - e^{-\beta\Delta}}{1 - e^{-\beta\hbar\omega}} \cdot \left[\frac{\hbar\gamma/\pi}{(\hbar\omega - \epsilon(\mathbf{Q}))^2 + (\hbar\gamma)^2} - \frac{\hbar\gamma/\pi}{(\hbar\omega + \epsilon(\mathbf{Q}))^2 + (\hbar\gamma)^2} \right] \quad (1)$$

where $\hbar\gamma$ is the spectral Half Width at Half Maximum (HWHM) and $\mathcal{A} \approx \hbar^2 \int \tilde{I}(\mathbf{Q}, \omega) \omega d\omega$ approximates the first moment in the limit where $\hbar\gamma \ll \epsilon(\mathbf{Q})$. With an

energy gap Δ , the phenomenological dispersion relation reads:

$$\epsilon(\mathbf{Q}) = \sqrt{\Delta^2 + \hbar^2(\delta Q_{\perp}^2 v_{\perp}^2 + \delta Q_{\parallel}^2 v_{\parallel}^2)} \quad (2)$$

Here $\delta Q_{\perp,\parallel} = |(\mathbf{Q} - \mathbf{Q}_0)_{\perp,\parallel}|$ is the projection of the deviation in wave vector transfer \mathbf{Q} from the critical wave vector \mathbf{Q}_0 perpendicular and parallel, respectively, to the $\hat{\mathbf{c}}$ -direction. We take the velocity to be isotropic within the tetragonal basal plane because the present data from the (*HO**L*) zone only is insensitive to potential in-plane anisotropy allowed by symmetry in the low *T* phases. The velocities used were determined from the *HO* phase, using the data in Fig. 1(b), and were found to be $v_H = v_K = v_{\perp} = 23.7(5)$ meV·Å and $v_L = v_{\parallel} = 32.5(7)$ meV·Å. Eq. 1 was convoluted with the 4D instrumental resolution function using RESLIB [18]. In order to extract reliable measurements of the energy gaps at both \mathbf{Q} -points, this fitting was performed for a variety of integration ranges in both *H* and *L*. The values of the gap, Δ , and width, $\hbar\gamma$, versus the integration area (in Å⁻²) were then extrapolated to the size of the resolution ellipse given by RESLIB. This allowed these parameters to be determined in a way that is only dependent on the instrumental resolution and not the integration range chosen to form the energy scan from the \mathbf{Q} -dependent data. The results are summarized in Table I. The error bars given for the values of Δ and $\hbar\gamma$ are a combination of the errors resulting from the RESLIB fits as well as the extrapolation described above.

Phase	Wavevector	\mathcal{A} (barn · meV)	Δ (meV)	$\hbar\gamma$ (meV)
PM	<i>Z</i>	1.00(8)	2.3(5)	2.4(4)
PM	Σ	3.0(2)	2.2(6)	1.8(2)
HO	<i>Z</i>	4.3(3)	2.3(4)	0.9(1)
HO	Σ	5.1(3)	4.2(2)	0.7(1)
AF	<i>Z</i>	5.8(6)	2.3(4)	0.9(2)
AF	Σ	6.1(1.5)	5.5(3)	0.7(1)

TABLE I: Results of fitting the data in Fig. 3 to the dispersion in Eq. 1. The determination of the errors for Δ and $\hbar\gamma$ are described in the text, while the error bars given for \mathcal{A} are a combination of the fitting error and the error from normalization, which was 6%.

In the *HO* phase, the excitation at the Σ point becomes gapped, with $\Delta = 4.2(2)$ meV. Upon entering the *AF* phase this gap increases to $\Delta = 5.5(3)$ meV, while the physical half width extracted from this analysis, $\hbar\gamma = 0.7(1)$ meV, is identical in the two phases. At the *Z* point the gap and width of the spectrum are also identical in the two phases. Note that the values for the gap and half width $\Delta = 2.3(4)$ meV and $\hbar\gamma = 0.9(2)$ meV are both larger than literature values [7] and this may be a result of the coarser \mathbf{Q} -resolution of the present measurement. The main difference in the scattering in the *AF* phase as compared to the *HO* phase is the increased gap at the Σ and the additional Bragg scattering

at (1,0,0). The first moment \mathcal{A} at the *Z* and Σ points are within error bars of the values in the *HO* phase, as may also be appreciated by comparing Fig. 3(b) and Fig. 3(c). The inset to Fig. 3(c) shows a transverse cut through the (1,0,0) elastic peak, the intensity of which corresponds to a moment size of 0.36(9) μ_B . This is evidence that the measurements were indeed conducted in the *AF* phase. Our observation of inelastic scattering at *Z* is not a surprise given the enhanced *AF* order. In previous, lower pressure work an inelastic peak was observed at *Z* for $P = 0.72$ GPa [10] but not for $P = 0.62$ GPa [13]. A possible explanation for all three neutron experiments under pressure is that the *Z* mode softens at the critical pressure and so falls within the elastic line in the lower pressure measurements. This would be consistent with recent high pressure Raman data [19].

We also note that the \mathbf{Q} -widths of the inelastic magnetic scattering in the *AF* and *HO* phases are similar and both broader than in the *PM* phase. The limited statistical quality of the *AF* phase data however, leaves it open for now whether or not there are coherent modes in the *AF* phase as in the *HO* phase. Between the paramagnetic and hidden order phases, transport and thermodynamic measurements indicate significant Fermi surface reconstruction [1, 20]. Resistivity [21], and quantum oscillation measurements [22], on the other hand, are much less affected by the *HO* to *AF* transition. Together with the similarities between the *HO* and *AF* spin correlations reported here, this suggests differences between these two phases of URu₂Si₂ are very subtle.

Apart from inducing or at least enhancing *AF* order, applied pressure shifts Σ -point intensity to slightly higher energies. This indicates a stabilization of *AF* order under hydrostatic pressure. Previous work interprets gapped excitations at the *Z* point as a signature of the *HO* phase [23]. However, the present data shows that entering the *AF* phase does not weaken or destroy either set of excitations. Likewise, pressure does not suppress the *HO* transition, but actually increases T_0 , before the *AF* phase emerges [24]. All these observations point to a significant kinship between the *HO* and *AF* phases of URu₂Si₂.

Acknowledgments

The authors would like to thank M.B. Stone for help with the data analysis. Work at IQM was supported by DoE, Office of Basic Energy Sciences, Division of Materials Sciences and Engineering under award DE-FG02-08ER46544. This work utilized facilities supported in part by the National Science Foundation under Agreement No. DMR-1508249. Research at McMaster University is supported by NSERC. T.J.W. acknowledges support from the Wigner Fellowship program at Oak Ridge National Laboratory.

-
- [1] T.T.M. Palstra, A.A. Menovsky, J. van den Berg, A.J. Dirkmaat, P.H. Kes, G.J. Nieuwenhuys and J.A. Mydosh. *Phys. Rev. Lett.* **55**, 2727 (1985).
- [2] C. Broholm, J.K. Kjems, W.J.L. Buyers, P. Matthews, T.T.M. Palstra, A.A. Menovsky and J.A. Mydosh. *Phys. Rev. Lett.* **58**, 1467 (1987).
- [3] D.A. Bonn, J.D. Garrett and T. Timusk. *Phys. Rev. Lett.* **61**, 1305 (1988).
- [4] W.J.L. Buyers, Z. Tun, T. Peterson, T.E. Mason, J.-G. Lussier, B.D. Gaulin and A.A. Menovsky. *Physica B* **199&200**, 95 (1994).
- [5] T.E. Mason, W.J.L. Buyers, T. Peterson, A.A. Menovsky and J.D. Garrett. *J. Phys.: Condens. Matter* **7**, 5089 (1995).
- [6] F. Bourdarot, A. Bombardi, P. Burlet, M. Enderle, J. Flouquet, P. Lejay, N.Kernavanois, V.P. Mineev, L.Paolasini, M.E. Zhitomirsky and B. Fåk. *Physica B* **359-361**, 986 (2005).
- [7] F. Bourdarot, S. Raymond and L.-P. Regnault. *Phil. Mag.* **94**, 3702 (2014).
- [8] S. Takagi, S. Ishihara, S. Saitoh, H.-i. Sasaki, H. Tanida, M. Yokoyama and H. Amitsuka. *J. Phys. Soc. Japan.* **76**, 033708 (2007).
- [9] C.R. Wiebe, J.A. Janik, G.J. MacDougall, G.M. Luke, J.D. Garrett, H.D. Zhou, Y.-J. Jo, L. Balicas, Y. Qiu, J.R.D. Copley, Z. Yamani and W.J.L. Buyers. *Nature Physics* **3**, 96 (2007).
- [10] D. Aoki, F. Bourdarot, E. Hassinger, G. Knebel, A. Miyake, S. Raymond, V. Taufour and J. Flouquet. *J. Phys. Soc. Jap.* **78**, 053701 (2009).
- [11] N.P. Butch, J.R. Jeffries, S. Chi, J.B. Leão, J.W. Lynn and M.B. Maple. *Phys. Rev. B.* **82**, 060408(R) (2010).
- [12] E. Hassinger, D. Aoki, F. Bourdarot, G. Knebel, V. Taufour, S. Raymond, A. Villaume and J. Flouquet. *J. Phys.: Conf. Ser.* **251**, 012001 (2010).
- [13] F. Bourdarot, E. Hassinger, S. Raymond, D. Aoki, V. Taufour, L.-P. Regnault and J. Flouquet. *J. Phys. Soc. Jap* **78**, 064719 (2010).
- [14] J.A. Rodriguez, D.M. Adler, P.C. Brand, C. Broholm, J.C. Cook, C. Brocker, R. Hammond, Z. Huang, P. Hundertmark, J.W. Lynn, N.C. Maliszewkyj, J. Moyer, J. Orndorff, D. Pierce, T.D. Pike, G. Scharfstein, S.A. Smee and R. Vilaseca. *Meas. Sci. Technol.* **19**, 034023 (2008).
- [15] N.P. Butch, M.E. Manley, J.R. Jeffries, M. Janoschek, K. Huang, M.B. Maple, A.H. Said, B.M. Leu and J.W. Lynn. *Phys. Rev. B.* **91**, 035128 (2015).
- [16] C.R. Wiebe, G.M. Luke, Z. Yamani, A.A. Menovsky and W.J.L. Buyers. *Phys. Rev. B* **69**, 132418 (2004).
- [17] C. Broholm, H. Lin, P.T. Matthews, T.E. Mason, W.J.L. Buyers, M.F. Collins, A.A. Menovsky, J.A. Mydosh and J.K. Kjems. *Phys. Rev. B* **43**, 12809 (1991).
- [18] A. Zheludev: ResLib 3.4 (Oak Ridge National Laboratory, (2007).
- [19] G. Blumberg. Private communication.
- [20] M.B. Maple, J.W. Chen, Y. Dalichaouch, T. Kohara, C. Rossel, M.S. Torikachvili, M.W. McElfresh and J.D. Thompson. *Phys. Rev. Lett.* **56**, 185 (1986).
- [21] M.W. McElfresh, J.D. Thompson, J.O. Willis, M.B. Maple, T. Kohara and M.S. Torikachvili. *Phys. Rev. B* **35**, 43 (1987).
- [22] E. Hassinger, G. Knebel, T.D. Matsuda, D. Aoki, V. Taufour and J. Flouquet. *Phys. Rev. Lett.* **105**, 216409 (2010).
- [23] A. Villaume, F. Bourdarot, E. Hassinger, S. Raymond, V. Taufour, D. Aoki and J. Flouquet. *Phys. Rev. B* **78**, 012504 (2008).
- [24] G. Motoyama, T. Nishioka and N.K. Sato. *Phys. Rev. Lett.* **90**, 166402 (2003).